電荷により時系列演算を行うスマートイメージセンサー

Integration-Time Based Computational Image Sensors

宮川　良平　　　金出　武雄*

Ryohei Miyagawa　　　Takeo Kanade*

（株）東芝　研究開発センター　　　カーネギーメロン大学*

Toshiba Corp. R&D Center　　Carnegie Mellon Univ.*

Integration-time based, time-domain computation provides an area-efficient way to process image information by directly handling photo-created charge during photo-sensing. We have fabricated and tested two integration-time based, time-domain computational image sensors. The first is a multi-integration time photo-receptor which uses different integration periods depending on light intensity. It exhibits a dynamic range for light intensity 128 times larger than that of a single integration period photoreceptor. The second is a CCD-based range-finding sensor which exploits two charge packets for light integration and detects the delay of the receiving light pulses. It has detected 15 cm distance difference.

I Introduction

Combining time-domain computation with *image-sensing* by means of VLSI is a powerful approach as demonstrated in motion detection,' change detection? and range-sensing[3] However, most previous work such as edge detection[4], smoothing[5-7], image compression* has focused on the spatial image computations after the image is formed. As such, these computations can be performed off-chip. In contrast, the time computation. which is performed while the image is being sensed, can get unique, rich, and otherwise not obtainable information. For example, time-domain computational sensors detect light intensity change[1,2] or the time at the peak intensity[3]. The time-domain computation is done in a single pixel element, so it can be implemented easily as a pixel-parallel image sensor.

Implementing computations in a small pixel area is still a very difficult problem. Charge domain Computation is an area efficient solution for this difficulty. Electric charge as a signal is directly processed in the Si substrate, as it is transferred in the CCD. There are many examples for charge-domain computation in image sensors[7-9]. The computations so far realized by those sensors, however, are mostly spatial computations, since the computational operands are charge packets, i.e. the result of integrating photo-created electrons/holes. Temporal computation in an image sensor by charge-domain processing is a very interesting concept.

We have realized this concept as integration-time based time-domain computational image sensors. We have fabricated and tested two computational sensors. One is a multiple integration-time photo-receptor; the other is a CCD-based time-of-flight range-finding photoreceptor. Our computational sensors perform time-domain computations by processing photo-electrons during the integration period. Computations occur by either throwing away fractions of photoelectrons for some period, or transferring and storing them in a different area. The resultant charge distribution represents the computational results.

2 Multiple Integration-time photoreceptor

The conventional photodiode integrates incident light for a fixed integration time. The disadvantage of the fixed integration time is that the sensor is easily saturated with strong light, so the dynamic range is limited. The multiple integration-time photoreceptor that we have developed does not simply integrate the photo-electrons for a fixed period. Instead, it has multiple integration periods, which are chosen depending on light intensity in order to avoid saturation. When the charge level becomes close to saturation, the integration is stopped at one of these integration periods, and the integration time is recorded. The

sensor can represent a wide range of light intensities using these two output signals.

2.1 Circuit Design

Figure 1 shows the circuit for the multiple integration-time (Multiple-IT) photoreceptor. It includes two photo-diodes. The photodiode-A (Pd-a) detects saturation and the photodiode-B (Pd-b) stores photo-electrons as a signal. Pd-a is connected to an inverter, which thresholds the
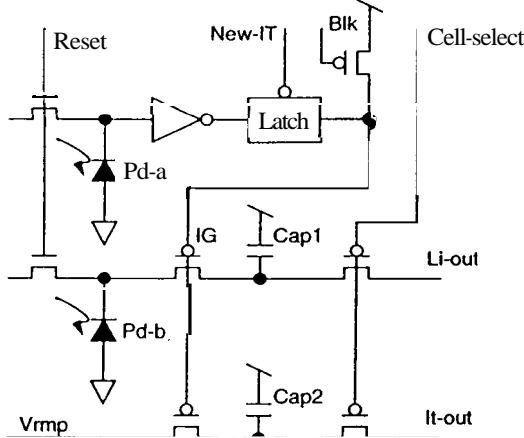
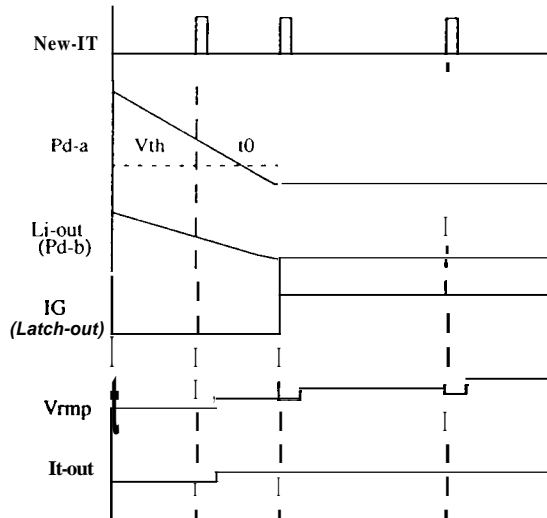Fig.1 Multiple integration time Photoreceptor

Fig. 2 Driving scheme for Multiple-IT photocell

Pd-a voltage. The output of the inverter is latched to control the gate connecting Pd-b to a storage capacitor (Cap1), which integrates signal charge. The latch output thus controls the integration periods. The latch output is also used for sample-holding a ramp voltage to record the integration period in the capacitor (Cap2).

Figure2 shows an example of the waveforms at various positions of the cell for the early part of a field period. The example is the case that the second integration period is chosen. The two photodiodes are first reset to a high volt-

age. Pd-a goes down, passes the first integration timing (It1), and then reaches the threshold for the inverter at t0. The inverter trips from low to high. However, the integration gate (IG) dose not change because the inverter output is latched. The integration timing pulse (New-IT) disables the latch and allows IG to change for a short period(1usec) at each integration timing. The latch-out goes high at the following integration timing (It2), the integration in Cap1 stops and the integration timing is recorded in Cap2 by sample-holding the ramp voltage (Vrmp). The ramp voltage is increased by a constant voltage after each integration timing. Each integration timing is arranged so that the following integration period is twice as long as the previous one. Turning on the blanking gate (Blk) forces the integration gate (IG) to close after one field period if the light intensity is too low for saturation. Eight integration timings were used. The n-th integration period is a $1/2^{8-n}$ of 1 field time.

2.2 Implementation and Experiment

The photoreceptor circuit was fabricated by MOSIS with the Orbit $2\mu m$ Analog process. The size of a photoreceptor is $109 \times 110\mu m$. We have tested the photoreceptor to
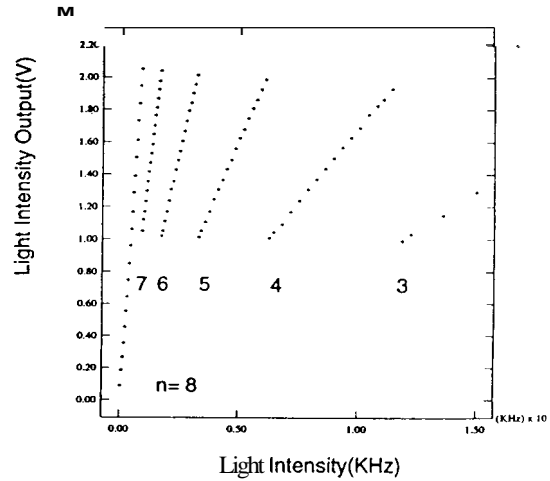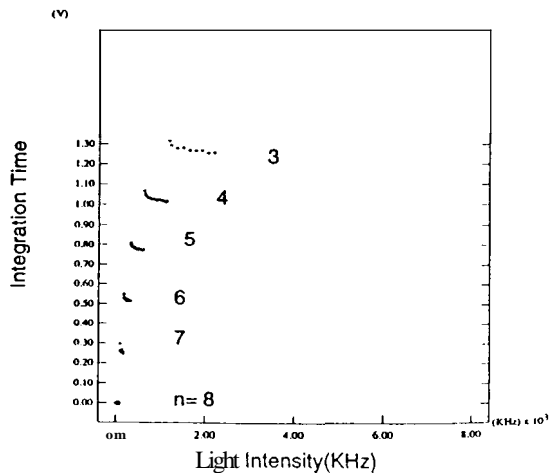
Fig. 3 Output1 vs. Light intensity

Fig 4 Output2 vs. Light intensity

investigate its behavior over a wide range of light intensities. We vaned the frequency of a LED light pulse which has a fixed width of 50nsec(keeping the LED on for 50nsec during each cycle) in order to precisely set the light intensity. The light intensity output (Li-out) and the integration time output (It-out) are plotted against light intensity in Fig.3 and Fig.4. The horizontal axes represent the light pulse frequency. Li-out increases linearly with light intensity in the largest integration period(n=8). It reaches a threshold and then switches to the second largest integration period(n=7). Li-out decreases by half with this transition and again increases linearly until it reaches the threshold again. Then, it switches to the next integration period(n=6) and so on. It-out moves to the next level with the transition of the integration period. We observed that It-out has the eight distinctive output levels corresponding to the integration periods.
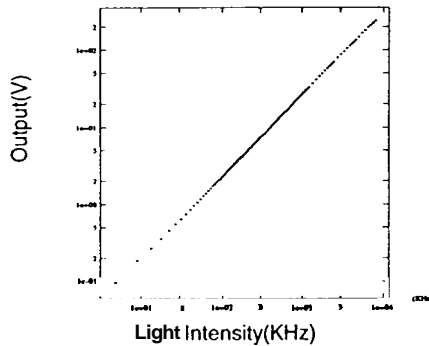

Fig.5 Reproduced outputs vs. Light intensity

Multiplying Li-out by 2^{8-n} according to the integration period, judged by It-out level, reproduces the actual light intensity level. The reproduced outputs are plotted against light intensity in Fig. **5.** There are eight segments of this graph, corresponding to the different integration periods. The transition from one integration period to the next is smooth and the output as a whole shows very good linearity over a wide range light intensity. The smallest integration period is one 128th of the largest integration time. Therefore, the dynamic range is 128 times larger than that of a single integration period photoreceptor.

3 CCD-based range-finding image sensor

One application of integration-time based computation is a sensor for active time-of-flight range measurement. The time-of-flight method estimates the distance to an object by measuring the delay of the received light pulses relative to the transmitted light pulses. Sandia researchers have built a range finding system by combining an image intensifier as a processor with a CCD imager **as** an integrator.'' We have realized such a range finder **as** a computational sensor.

3.1 Range-sensing Operation

Fig. 6 illustrates the principle to detect the light pulse delay. Light pulses modulated at 10MHz are transmitted towards an object. The received light pulses have a delay depending on the distance to the object. The delay time is

measured as a phase shift ($\Delta\phi$) by the two sensing periods (IT1, IT2). The two signals (L1,L2) representing the light intensities for IT1 and IT2 can detect the phase shift.

We have implemented this principle by a CCD transfer mechanism. Figure 7 shows the cross-sectional sketch for a test cell of CCD based range-finding sensor. The lower part of the figure is the potential diagram of CCD channels in the photoreceptor. The sensor operation is as follows. 10MHz light pulses come through an aperture over photo-gate (PG) and photo-electrons are created under PG. There are two window gates (WG1,WG2) one on
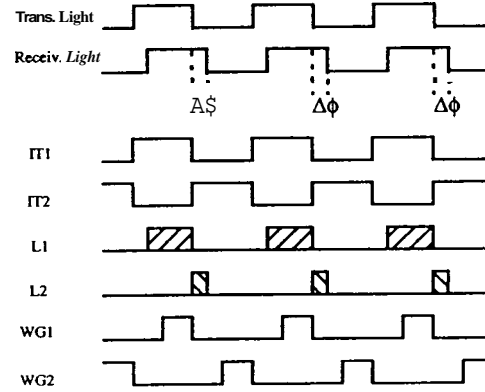

Fig. 6 Principle for detecting light pulse delay

each side of PG to control which direction the photo-electrons are transferred. WG1 and WG2 are turned on alternately at 10MHz, that makes the two integration period (IT1, IT2) **as** shown in Fig.6. Therefore, some portion (L1) of the light pulse in one clock time is stored under the storage gate **1** (SGI) and the rest (L2) is stored under the storage gate 2 (SG2). The portion is determined by the temporal position of the light pulse relative to the window gate pulses. Conversely. the storage charge difference between SGI and SG2 gives the light delay relative to the window gate timing. The operation of distributing charge to the two packets repeats with a series of light pulses for a certain period to integrate enough signal charge under the storage gates. The integrated charges are transferred through OG to the detection nodes (FD1,FD2) which are connected to output amplifiers.

3.2 Test Cell Experiment

We have fabricated a test cell and verified its operation. The chip was illuminated directly by a light pulse, which was created by a LED, and whose delay time was controlled by a programmable delay line. The wavelength of the LED was 592nm and its response time was 13nsec, fast enough for the 10MHz drive. The least step for the delay line was 0.25 nsec. The measurement results were plotted against the delay time in Fig.8 and Fig.9. Output1 first increased with the delay time and then decreased. Output2 was the exact opposite of Output1. The sum of Output1 and Output2 was almost the same. Output1 and
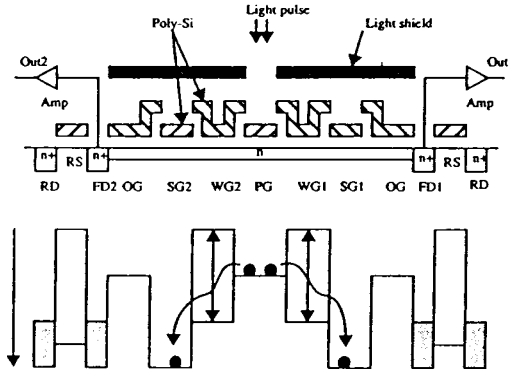
Fig. 7 Cross-sectional sketch and potential diagram
for CCD based range finding photoreceptor

Output2 can be regarded **as** in-phase and out-of-phase components, respectively. The light pulse came in-phase with increasing delay and was fully in-phase at the peak of Output1. It went out-of-phase after the peak. This result has shown that the photo-electrons were successfully differentiated according to the window periods. Note that the Output2 value at the bottom was much larger than zero,
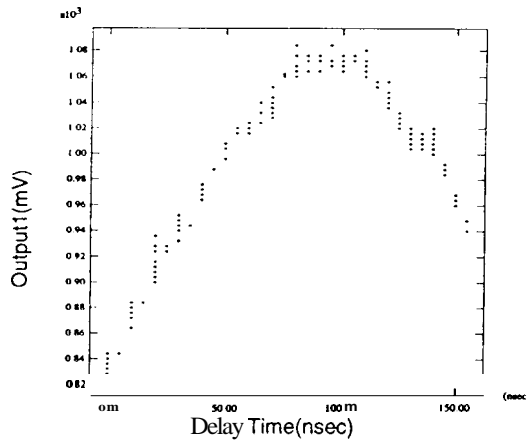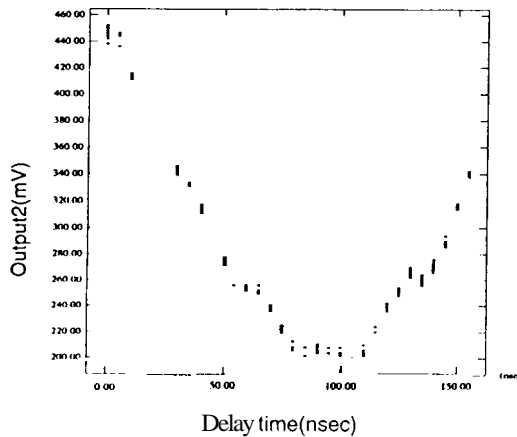

Fig. 8 Output1 vs. Delay time

Fig.9 Output2 **vs.Delay** time

	W1:off	W2:off
Output1	202 mV	1158 mV
output2	1134 mV	173 mV

though the light pulse was fully in-phase. In order to investigate this phenomena, we measured both outputs turning off one window gate pulse and with 0 nsec delay time. The result was listed in the table below. Both outputs have significant voltage output without the window gate pulses. These value were very close. This means that the photoelectrons created in deep depth directly entered each storage area, regardless the window gate operation. The cause of this small difference could be a small shift of the aperture from the center of two storage gates. This direct leakage effect needs to be taken into account when calculating the range.

The range estimation can be done **as** follows. Let $Q1$ and $Q2$ be photo-charges transferred by the window gate 1 and 2, respectively. Let $Q1l$ and $Q2f$ the photo-charges leaked into the storage gate 1 and 2, respectively. The light pulse phase shift determines the relative distance. Therefore, the relative range an be estimated by

$$Range = \frac{1}{4} \cdot \left(\frac{Q1 + Q1l - Q2 - Q2l}{Q1 + Q1l + Q2 + Q2l} \right) \cdot \frac{c}{PulseWidth}$$

All the charges are linear to the total charge(Qt). It is assumed $Q1l$-$Q2l$ $\ll$ Qt. We can simplify this expression by noting:

$$\left(\frac{Q1 + Q1l - Q2 - Q2l}{Q1 + Q1l + Q2 + Q2l} \right) \cong \left(\frac{Q1 - Q2}{Q1 + Q2} \right) \cdot \left(\frac{Q1 + Q2}{Qt} \right)$$

(Q1-Q2)/(Q1+Q2) represents the real light pulse position. The estimated range is shown **as** follows.

$$Range = RealRange \cdot r$$

where r =(Q1+Q2)/Q

t . The value of r was 0.86 with the data listed in the previous table. Therefore, the leakage charge dose not significantly influence on the range estimation

3.3   1 D **Array** Range-finding Sensor

Figure 10 shows the structure for a range-finding 1D-array sensor. The linear sensor **has** very similar cell structure to the test photo-cell. The difference is that the line sensor transfers both signal charges in the same direction to a detection node after signal charge integration. All the gates function **as** a 4-phase CCD when transferring the signal charges. The signal charges which reach their detection nodes **are** read-out by source-followers. Each detection node is serially scanned by a shift-register. **A** 32 pixel line-sensor was fabricated by MOSIS with the Orbit $2\mu m$ Analog process. The size of each pixel is 36 **x** $36\mu m$.

We mounted camera optics on the line sensor and placed a white **box** at various distances. The sensor outputs were observed using a digital oscilloscope. The observed waveforms were averaged over 32pixels. The averaged data were used to estimate the range by using the equation

above in the previous section, We found the sensor sensitivity was very low because of the thick 6000A poly silicon PG, *so* the signal charges were integrated for 1.06sec. There was also significant dark current with the long integration period, which caused a lot of noise. This is one of the reasons that the outputs of the 32 pixels were averaged. The estimated distance is plotted in Fig11. The horizontal axis is the distance of the object from a certain point.

Estimated distance increases linearly with real distance for the range of 10-40cm and **for** 40-70cm. There was a gap in the curve. Light intensity was intentionally changed between the two curves tocompensate **for** an impefect plane light source. The reason for the gap in the curve may be that the detection node is not a linear capacitor.
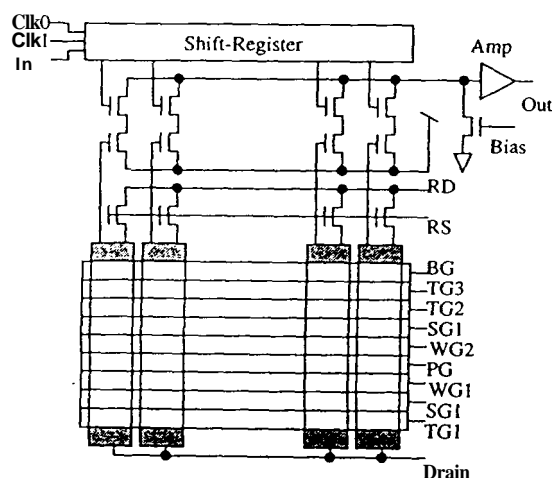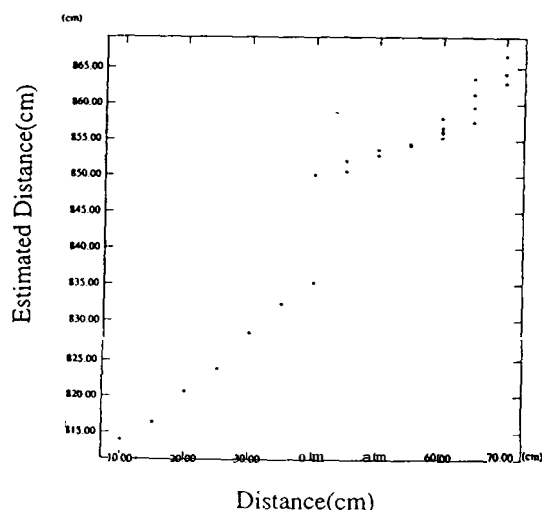

Fig.10 Range-finding line sensor structure

Distance(cm)

Fig. 11 Range estimation

4　Conclusion

The two time-domain computational photoreceptors have been fabricated and tested. Their unique capabilities have shown that the time-domain computation at the level of phototransduction is a powerful methodology.

References

[1]　T.Delbruck, "Silicon retina with correlation-based, velocity-tuned pixels," IEEE Trans. on Neural Network, vol.4 pp.529-541 (1993)

[2]　T.Delbruck and C.A.Mead, "Time-derivative adaptive silicon photoreceptor array," Proc. SPIE vol. 1541, pp.92-99

[3]　A.Gruss et. al, "Integrated sensor and range-finding analog signal processor." IEEE J. Solid-state circuit vol.26 pp.184-190 (1991)

[4]　J, G. Harris et. al, "Two dimensional analog VLSI circuit for detecting discontinuities", Science, Vol.248, pp1209-1211. (1990)

[5]　P. C. Yu et. al, "CMOS resistive **fuses** for image smoothing and segmentation", IEEE J. Solid-State Circuits, Vol.27, pp 545-552, (1992)

[6]　H. Kobayashi et. al, "An Analog CMOS Network for gaussian convolution with embedded image sensing", in Tech. Digest ISSCC 1990, pp216-217

[7]　C. L. Keast et. al, "A CCD/CMOS- based imager with integrated focal plane signal processing", IEEE J. Solid-state Circuit Vol.28, pp431-437, (1993)

[8]　S. E. Kemeny et. al, "CCD forcal-plane image reorganization processors for lossless image compression", LEEE J. Solid-state Circuit, Vol.27, pp398-405, (1992)

[9]　W. Yang and A. Chiang, "A **full** fill-factor CCD imager with integrated signal processors", in Tech. Digest ISSCC 1990, pp218-219

[IO]　J. P. Anthes et. al, "Non-scanned LADAR imaging and application", in Proc SPIE Vol.1936, pp.11-21 (1993)